Materials Science and Engineering A 519 (2009) 147–154

Contents lists available at ScienceDirect

Materials Science and Engineering A

journal homepage: www.elsevier.com/locate/msea

On the mechanism of unstable plastic flow in an austenitic FeMnC TWIP steel

T.A. Lebedkina[a], M.A. Lebyodkin[b,*], J.-Ph. Chateau[c], A. Jacques[c], S. Allain[d]

[a] Institute of Solid State Physics, Russian Academy of Sciences, 142432 Chernogolovka, Russia
[b] LPMM, Université Paul Verlaine – Metz/CNRS, Ile du Saulcy, 57045 Metz Cedex 01, France
[c] LPM, Ecole des Mines/CNRS, Parc de Saurupt, 54042 Nancy Cedex, France
[d] Arcelormittal Maizières Research SA, Voie Romaine, BP 30320, 57283 Maizières les Metz, France

ARTICLE INFO

Article history:
Received 19 December 2008
Received in revised form 26 April 2009
Accepted 28 April 2009

Keywords:
High manganese austenitic steel
Jerky flow
Deformation inhomogeneities
TWIP
Dynamic strain aging

ABSTRACT

The complex character of plastic deformation of the austenitic steel Fe22Mn0.6C is studied at room temperature with the aid of high-frequency local extensometry. It is shown that the plastic flow instability, associated with fluctuations of the flow stress, results from quasi-continuous propagation of deformation bands along the specimen axis. This propagation mode is dominant in the entire range of the applied strain-rate from $2.1 \times 10^{-5}\,s^{-1}$ to $10^{-1}\,s^{-1}$. Such behavior differs from that of various alloys deforming via dislocation glide under conditions of dynamic strain ageing (Portevin-Le Chatelier effect), which is characterized by a transition from a repetitive occurrence of static deformation bands at lower strain rates to a relay-race and, finally, quasi-continuous deformation band propagation at higher strain rates. The unusual behavior of the deformation bands bears evidence to a particular kind of instability in the investigated steel. A possible role of deformation twins in the observed dynamics of plastic instability is discussed.

1. Introduction

The plastic deformation of steels with high manganese content, such as Fe22Mn0.6C (wt.%), exhibits macroscopic plastic instabilities in a wide range of strain-rate and temperature and is characterized by stress fluctuations of various shapes on the stress–strain curve. The resulting deformation curves present different morphologies depending on temperature. Such variance is consistent with the temperature dependence of the microscopic mechanisms of plastic flow of this material, which depend on stacking fault energy (SFE) [1–3]. Indeed, when the deformation temperature is decreased from 673 K down to 77 K, dislocation glide, twinning plus glide, and martensitic transformation plus glide (ε-martensite with h.c.p. lattice crystallographic structure) are successively observed in accordance with the diminishing SFE [4]. Therefore, it is natural to suggest that the instabilities observed under various deformation conditions can be governed by different microscopic mechanisms. These mechanisms are not known yet, perhaps, with an exception for a temperature interval above 150–200 °C, where the dynamical strain aging of dislocations due to carbon atoms may lead to the Portevin-Le Chatelier effect [5,6]. However, this problem is of interest for both practical applications, since the instabilities impede the processing of these steels, which otherwise possess remarkable mechanical features [7,8], and for understanding the basic problem of the deformation mechanisms leading to instability of the uniform plastic flow.

At room temperature, the studied FeMnC steel is fully austenitic, with a sufficiently low SFE to promote twinning, which enters into the competition with dislocation glide, as reflected in the notion of twinning-induced plasticity (TWIP) [7]. As a matter of fact, this peculiar feature is at the origin of this steel attraction for industry because it provides a high strain hardening rate leading simultaneously to high ductility and tensile strength. It is known that the formation of twins may be accompanied with pronounced stress fluctuations, although it usually concerns low-temperature deformation [9]. However, the instabilities observed in this steel at room temperature are often tentatively ascribed to the PLC effect [10]. This assumption is based on the observation of the negative strain-rate sensitivity (SRS) of the flow stress and a thermally activated character of plastic deformation. Nevertheless, the diffusion coefficient of carbon in austenite appears to be too low at room temperature to account for the PLC effect [11]. On the other hand, it is known that the negative SRS is not a peculiar feature of the PLC effect only. It also emerges for distinct mechanisms, e.g. for thermo-mechanical instability, which is known to be caused by local overheating of specimens deformed at low temperatures [12]. Moreover, the thermo-mechanical instability demonstrates features in common with the PLC effect, as far as the morphology of the deformation curves and the statistics of stress jumps are concerned [13]. This example proves that neither the behavior of the

* Corresponding author. Tel.: +33 03 87315401.
E-mail addresses: lebedkin@univ-metz.fr, lebma@mail.ru (M.A. Lebyodkin).

0921-5093/$ – see front matter © 2009 Elsevier B.V. All rights reserved.
doi:10.1016/j.msea.2009.04.067

SRS nor the similarity of the morphology of deformation curves is a sufficient criterion for distinguishing between various instability mechanisms.

In order to provide a further insight into the mechanism of plastic instability in austenitic TWIP steels at room temperature, we study the local strain distribution during tensile deformation of FeMnC samples using high-rate extensometry technique [14]. This paper is organized as follows. Section 2 outlines experimental details and data processing. Section 3 describes experimental data on the macroscopic tensile behavior of the studied steel and the concomitant evolution of the local strain heterogeneity. The overall discussion, including the comparison of the evolution of the strain distribution to salient features of PLC bands, is given in Section 4. Finally, Section 5 highlights hypotheses on which mechanisms are able to lead to the observed plastic instabilities.

2. Experimental procedure

Flat tensile specimens with a gauge section 60 mm × 12.6 mm × 1.25 mm in size were prepared from a Fe–22 wt.% Mn–0.6 wt.% C steel, with approximately 3 μm grain size. Mechanical tests were performed at room temperature with a constant crosshead speed. The nominal value of the imposed strain-rate $\dot{\varepsilon}_a$, corresponding to the initial specimen length, was varied in the range from $2.08 \times 10^{-5}\,s^{-1}$ to $2.5 \times 10^{-2}\,s^{-1}$. Besides, several tests were performed on samples fabricated separately but with the same nominal composition and grain structure. These specimens with dimensions 80 mm × 5.4 mm × 0.6 mm were tested in a strain-rate range from $2.2 \times 10^{-5}\,s^{-1}$ to $8 \times 10^{-3}\,s^{-1}$ [2]. Using such specimens, one test was performed with the aid of a pyrometry technique to visualize strain localization at the strain-rate $\dot{\varepsilon}_a = 10^{-1}\,s^{-1}$ [11].

In order to conduct local extensometry, one surface of the specimen was painted black, and somewhat 10 white marks of 1 mm in width were superimposed on the black layer normal to the longitudinal axis as illustrated in Fig. 1. The distance between the marks was approximately equal to 1 mm. The resulting sequence of black and white stripes formed a set of about twenty 1 mm long extensometers, in the center of the 60 mm gauge length. The positions of the transitions between black and white marks during the sample deformation were followed using a high resolution 1D CCD camera with a recording frequency of 10^3 Hz and a pixel size of 1.3 μm. The camera was fixed relative to the fixed crosshead. It aimed at the specimen axis in order to avoid any cross-section rotation effect, although negligible in the case of polycrystals. As a matter of fact, the deformation of the samples appeared to be uniform on average in all tests, so that no noticeable rotation effect was observed before ultimate necking. The camera allowed continuous recording during an interval of 600 s, which covered the entire test duration at higher strain rates of $\dot{\varepsilon}_a > 1.5 \times 10^{-3}\,s^{-1}$. Consequently, the strain dependence of various parameters of the strain pattern could be built. For lower $\dot{\varepsilon}_a$ values, it was possible to survey only portions of tests. In this case, the measurements were repeated several times during the test in order to evaluate the local deformation kinetics qualitatively.

To estimate the continuous work hardening rate, $\Theta = \partial\sigma(\varepsilon, \dot{\varepsilon})/\partial\varepsilon$, the deformation curves obtained at different imposed strain rates were fitted with polynomials in the strain intervals from $0.005 \le \varepsilon_{\log} \le 0.5$–$0.6$, to eliminate stress fluctuations. The estimation of Θ evolution with strain was then obtained by deriving the fitting function. The evolution of the local strain values were calculated from the displacements measured by the CCD camera:

$$\varepsilon_i(t) = \ln \frac{x_{i+2}(t) - x_i(t)}{x_{i+2}(0) - x_i(0)}, \quad (1)$$

where x_i is the coordinate of the ith transition. In this equation, every second section is taken in order to avoid a possible artefact due to unequal sensitivity of the camera to black–white and white–black transitions. During performing the mechanical test, some extensometers leave the camera's field of vision, some others will enter into it. For this reason, the initial time in Eq. (1) was usually not selected at the beginning of deformation, but at a later instant, in order to seize the largest number of extensometers. In this case, only the relative changes in the local strain values were meaningful. In addition to $\varepsilon_i(t)$ local strain rates $\dot{\varepsilon}_i(t)$ were calculated by deriving the $\varepsilon_i(t)$ dependence after preliminary reduction of digital noise with the aid of a running average technique. The construction of strain maps, $(t, x_i(0), \varepsilon_i(t))$, and the respective strain-rate maps, $(t,\ x_i(0),\ \dot{\varepsilon}_i(t))$, allowed visualization of the evolution of the local strain field and, particularly, provided a simple tool to distinguish between the band propagation and localization. These maps, together with the $\varepsilon_i(t)$ dependence, provide evaluation of the band velocity, V_b, band width, w, and the associated strain, ε_b. As the maps refer to the gauge length of the local extensometers at the initial time, the values of V_b and w are corrected taking the sample elongation into account. Other kinds of data representations, though less illustrative, were also used to evaluate the deformation band parameters. For example, the axial strain distribution profiles $\varepsilon_i(x_i)$ were calculated at subsequent time instants. All methods provided close values for the deformation band parameters.

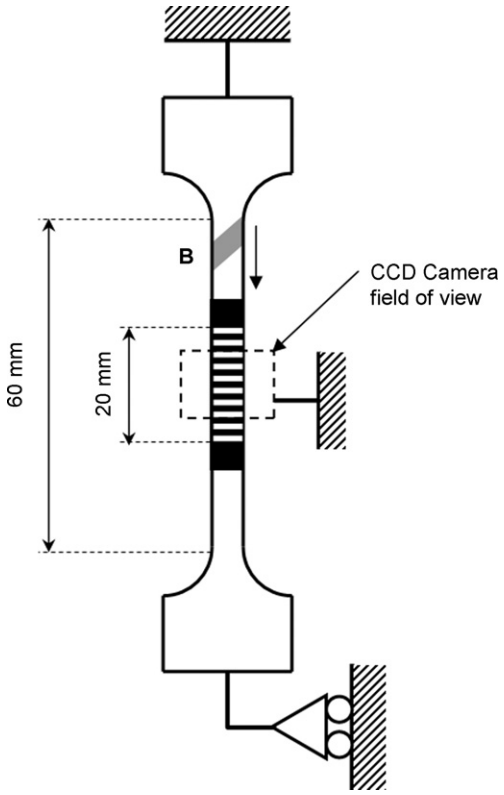

Fig. 1. Scheme of the experimental setup. The black and white stripes depict the set of extensometers painted on its surface. A deformation band (B) propagates from the top to the bottom of the specimen.

3. Results

3.1. Macroscopic behavior

Fig. 2 shows some representative true stress–strain tensile curves recorded at different imposed strain rates. A negative SRS occurs in the entire strain-rate range investigated as described in Ref. [11] for strain rates up to $1\,s^{-1}$. A rough evaluation of the SRS using a relationship $S \approx \Delta\sigma/\ln(\dot{\varepsilon}_a^2/\dot{\varepsilon}_a^1)$ for pairs of deformation